

Orbital Magnetism in Three-Dimensional Quantum Dots

Takeru SUZUKI , Hiroshi IMAMURA, Masahiko HAYASHI and Hiromichi EBISAWA
*Graduate School of Information Sciences,
 Tohoku University, Sendai 980-8579*

We study orbital magnetism in a three-dimensional (3D) quantum dot with a parabolic confining potential. We calculate the free energy of the system as a function of the magnetic field and the temperature. By this, we show that the temperature-field plane can be classified into three regions in terms of the characteristic behavior of the magnetization: the Landau diamagnetism, de Haas-van Alphen oscillation and mesoscopic fluctuation of magnetization. We also calculate numerically the magnetization of the system and then the current density distribution. As for the oscillation of the magnetization when the field is varied, the 3D quantum dot shows a longer period than a 2D quantum dot which contains the same number of electrons. A large paramagnetism appears at low temperatures when the magnetic field is very weak.

PACS numbers:

Orbital magnetism of a bulk system appears as the Landau diamagnetism (LD). In the past, Landau's work has provoked discussion regarding his treatment of boundary [1, 2] and the effects of boundary on the orbital magnetism have been studied by many people. [3, 4] Recently, two-dimensional (2D) quantum dots have become experimentally available with the capability of controlling the dots' size, shape and number of electrons. [5, 6, 7] Stimulated by experimental development, many theorists have been studying on 2D quantum dots with parabolic confining potentials. In particular, Ishikawa and Fukuyama (IF) [3] have claimed that the temperature-field (T - B) plane can be classified into three regions in terms of the characteristic behavior of the magnetization $M(T, B)$: the LD, de Haas-van Alphen (dHvA) oscillation and mesoscopic fluctuation (MF) of magnetization. Such magnetic behavior is mainly governed by the energy levels near the Fermi level of the system. In the case of 3D quantum dots, the additional degree of freedom makes the density of states larger than that of 2D quantum dots. Hence, it is expected that the temperature affects the magnetization more easily, which changes the magnetic behavior to some extent and possibly invalidates the classification.

In this letter, we present our study on the orbital magnetism of 3D quantum dots. We consider noninteracting electrons confined in a parabolic potential and calculate analytically the free energy Ω of the system. Thereby, we show that the temperature-field plane can still be classified into the above three regions in terms of the characteristic behavior of the magnetization, $M(T, B) = -\partial\Omega/\partial B$. In order to confirm this classification, we calculate numerically the magnetization of the system and then the current density distribution. In addition to the consistency between the analytical and numerical calculations, we report some remarkable findings of our numerical calculation. Hereafter, we set the fundamental constants as $\hbar = c = k_B = 1$.

We consider spinless electrons of effective mass m and charge $-e$ confined in a spherical quantum dot with a

parabolic confining potential in a uniform magnetic field \mathbf{B} . The total Hamiltonian H of the system is given by the sum of single electron Hamiltonians as

$$H = \sum_{i=1}^N \left\{ \frac{1}{2m} [-i\nabla_i + e\mathbf{A}(\mathbf{r}_i)]^2 + \frac{m}{2}\omega_3^2 \mathbf{r}_i^2 \right\}, \quad (1)$$

where N is the total number of electrons, and \mathbf{A} is a vector potential satisfying $\mathbf{B} = \text{rot}\mathbf{A}$. The last term represents the confining potential, where ω_3 parametrizes the strength of the isotropic confinement.

The eigenstates of the single electron Hamiltonian comprise the Fock-Darwin states in the x - y plane [3] and the eigenstates of a harmonic oscillator in the z -direction parallel to \mathbf{B} . In the cylindrical coordinate (ρ, ϕ, z) , the eigenfunction ψ is given by

$$\psi_{n\alpha\nu}(\mathbf{r}) = (2\pi)^{-\frac{1}{2}} \exp(i\alpha\phi) R_{n\alpha}(\rho) Z_\nu(z), \quad (2)$$

where n, α, ν are integers and $n, \nu \geq 0$. (n, α, ν) consists of a set of quantum numbers. $R_{n\alpha}(\rho)$ is the radial wave function of the Fock-Darwin state specified by (n, α) and $Z_\nu(z)$ is the ν -th eigenfunction of the harmonic oscillator. The eigenenergy $E_{n\alpha\nu}$ is given by

$$E_{n\alpha\nu} = \left(n + \frac{1}{2}\right) \omega_1 + |\alpha| \omega_2 + \left(\nu + \frac{1}{2}\right) \omega_3, \quad (3)$$

$$\omega_1 = \sqrt{\omega_B^2 + 4\omega_3^2}, \quad (4)$$

$$\omega_2(\pm) = \omega_\pm = \frac{1}{2}(\omega_1 \pm \omega_B), \quad (5)$$

where ω_B denotes the cyclotron frequency, $\omega_B = eB/m$. In eq. (5), the characteristic frequency $\omega_2 = \omega_2(\sigma)$ depends on the sign σ ($= \pm$) of the angular momentum α . Hereafter, we set ω_3 as the energy unit, though we keep the symbol ω_3 in the several equations below for clarity.

The magnetization M of the entire system is given by $M = -(\partial\Omega/\partial B)_{T\mu}$, [8] where T is the temperature, μ is the chemical potential, and Ω is the free energy of the system, $\Omega = -T \sum_{n\alpha\nu} \ln\{1 + \exp[(\mu - E_{n\alpha\nu})/T]\}$. By means of the Poisson summation formula, [9] the triple

sum with respect to n, α, ν is transformed into another triple sum, $\Omega = \sum_{p,q,r=-\infty}^{\infty} \Omega_{pqr}$, where Ω_{pqr} is expressed as the Fourier integral which we can calculate analytically by assuming $\mu \gg T$ and $\mu \gg \omega_B$. With these calculations carried out, the free energy Ω is given as follows,

$$\Omega \approx \Omega_0 + \tilde{\Omega}, \quad (6)$$

$$\Omega_0 = -\frac{1}{24}\mu^4 + \left(\frac{1}{48}\omega_B^2 - \frac{\pi^2}{12}T^2 + \frac{1}{16}\right)\mu^2, \quad (7)$$

$$\tilde{\Omega} = \sum_{i=1}^3 \Omega_i = \sum_{i=1}^3 \sum_{\sigma=\pm} \sum_{p=1}^{\infty} \Omega_i^{\sigma}(p), \quad (8)$$

$$\Omega_i^{\sigma}(p) = Q_i^{\sigma}(p) \Psi(2p\pi^2T/\omega_i) \cos(2p\pi\mu/\omega_i), \quad (9)$$

$$Q_i^{\sigma}(p) = -\frac{(-1)^{ip}\omega_i^3}{8\pi^4 p^4 \omega_j \omega_k} - \sum_{q=1}^{\infty} \frac{(-1)^{ip}}{4\pi^4 p^2} \left[\frac{(-1)^{jq}\omega_i^3 \omega_j}{\omega_k(p^2\omega_j^2 - q^2\omega_i^2)} + \frac{(-1)^{kq}\omega_i^3 \omega_k}{\omega_j(p^2\omega_k^2 - q^2\omega_i^2)} \right] - \sum_{q=1}^{\infty} \sum_{r=1}^{\infty} \frac{(-1)^{ip+jq+kr}\omega_i^3 \omega_j \omega_k}{2\pi^4(p^2\omega_j^2 - q^2\omega_i^2)(p^2\omega_k^2 - r^2\omega_i^2)}, \quad (10)$$

where $\Psi(x) = x/\sinh(x)$, and in eq.(10), the coefficients $Q_1^{\sigma}, Q_2^{\sigma}, Q_3^{\sigma}$ take the set of indices $(i, j, k) = (1, 2, 3), (2, 3, 1), (3, 1, 2)$, respectively. The summation in eq.(10) is executed further and we obtain

$$Q_1^{\sigma}(p) = -\frac{(-1)^p \omega_1}{8\pi^2 p^2 \tan(\pi p \omega_2/\omega_1) \sin(\pi p \omega_3/\omega_1)}, \quad (11)$$

$$Q_2^{\sigma}(p) = -\frac{\omega_2}{8\pi^2 p^2 \sin(\pi p \omega_3/\omega_2) \sin(\pi p \omega_1/\omega_2)}, \quad (12)$$

$$Q_3^{\sigma}(p) = -\frac{(-1)^p \omega_3}{8\pi^2 p^2 \sin(\pi p \omega_1/\omega_3) \tan(\pi p \omega_2/\omega_3)}. \quad (13)$$

The free energy Ω_0 in eq. (7) is the nonoscillating part with respect to the magnetic field, while $\tilde{\Omega} = \Omega_1 + \Omega_2 + \Omega_3$ in eq. (8) represents the oscillating part of the total free energy Ω . For the oscillating part, the free energy $\Omega_1 = \sum_{\sigma} \sum_p \Omega_1^{\sigma}(p)$ vanishes because $\sum_{\sigma} \Omega_1^{\sigma}(p) \propto \sum_{\sigma} Q_1^{\sigma}(p)$ is identically zero due to eq. (5). As for Ω_2 , $\Omega_2^{\pm}(p)$ has the oscillating factor, $\cos(2p\pi\mu/\omega_{\pm})$, in eq. (9) as a function of the field parameter ω_B since ω_{\pm} varies monotonically with respect to ω_B . Although the remaining factor $Q_2^{\pm}(p)$ in $\Omega_2^{\pm}(p)$ also oscillates by $\sin(\pi p \omega_3/\omega_{\pm}) \sin(\pi p \omega_1/\omega_{\pm})$ in eq. (12), we can neglect this oscillation, compared with $\cos(2p\pi\mu/\omega_{\pm})$, since we can assume $\omega_3 \ll \mu$ for the sufficiently large size of the system and also $\omega_1 \ll \mu$ due to the assumption, $\mu \gg \omega_B$. As for Ω_3 , $\Omega_3^{\sigma}(p)$ in eq. (9) has only a negligible oscillation caused by $\sin(\pi p \omega_1/\omega_3) \tan(\pi p \omega_2/\omega_3)$ in eq. (13), because $\cos(2p\pi\mu/\omega_3)$ is independent of the magnetic field. Consequently, Ω_2 is dominant in eq. (8) in terms of the oscillation of magnetization. Hereafter, we write the effective part of the free energy $\tilde{\Omega}$ as

$$\tilde{\Omega}_{\text{eff}} = \sum_{\sigma=\pm} \sum_{p=1}^{\infty} Q_2^{\sigma}(p) \Psi(2p\pi^2T/\omega_{\sigma}) \cos(2p\pi\mu/\omega_{\sigma}), \quad (14)$$

where $\omega_{\sigma} = \omega_2(\sigma)$.

It should be noted, however, that eqs. (11)-(13) have spurious divergent singularities when ω_i/ω_j is a rational number. To eliminate such divergences, we rewrite $\tilde{\Omega}$ as defined in eqs. (8)-(10), by rearranging terms, into

$$\tilde{\Omega} = \sum_{\sigma=\pm} \left(\sum_{p=1}^{\infty} \hat{\Omega}_p^{\sigma} + \sum_{p,q=1}^{\infty} \hat{\Omega}_{p,q}^{\sigma} + \sum_{p,q,r=1}^{\infty} \hat{\Omega}_{p,q,r}^{\sigma} \right), \quad (15)$$

$$\hat{\Omega}_p^{\sigma} = -\frac{(8\pi^4)^{-1}}{\omega_1 \omega_2 \omega_3} \sum_{i=1}^3 (-1)^{ip} \frac{Y(p/\omega_i)}{(p/\omega_i)^4}, \quad (16)$$

$$\hat{\Omega}_{p,q}^{\sigma} = -\frac{(4\pi^4)^{-1}}{\omega_1 \omega_2 \omega_3} \sum_{(i,j)} (-1)^{ip+jq} \frac{\frac{Y(p/\omega_i)}{(p/\omega_i)^2} - \frac{Y(q/\omega_j)}{(q/\omega_j)^2}}{(p/\omega_i)^2 - (q/\omega_j)^2}, \quad (17)$$

$$\hat{\Omega}_{p,q,r}^{\sigma} = -\frac{(2\pi^4)^{-1}}{\omega_1 \omega_2 \omega_3} (-1)^{p+r} \times \frac{\frac{Y(p/\omega_1) - Y(r/\omega_3)}{(p/\omega_1)^2 - (r/\omega_3)^2} - \frac{Y(q/\omega_2) - Y(r/\omega_3)}{(q/\omega_2)^2 - (r/\omega_3)^2}}{(p/\omega_1)^2 - (q/\omega_2)^2}, \quad (18)$$

where $Y(x) = \Psi(2\pi^2Tx) \cos(2\pi\mu x)$, and in eq.(17), the index (i,j) takes $(1,2), (2,3)$ and $(3,1)$. Equations (16)-(18) are apparently free from divergences. It is expected that as the temperature T rises, the total amplitude of oscillation is rapidly suppressed by the exponentially decreasing factor, $\Psi(2p\pi^2T/\omega_i) \sim (4p\pi^2T/\omega_i) \exp(-2p\pi T/\omega_i)$.

At sufficiently high temperatures, it is expected that Ω_0 in eq. (7) makes a dominant contribution to the total free energy Ω , and the magnetization M_0 is given by

$$M_0/\mu_B = -2(\partial\Omega_0/\partial\omega_B)_{T\mu} = -\frac{1}{12}\mu^2\omega_B, \quad (19)$$

where $\mu_B = e/(2m)$ is the Bohr magneton. The magnetization M_0 is negative and its absolute value increases linearly with increasing ω_B , which is characteristic of the LD in a bulk system. [9] On the other hand, at low temperatures, by using the free energy $\tilde{\Omega}_{\text{eff}}$ in eq. (14), we obtain an oscillating part of the magnetization, $\tilde{M}/\mu_B = -2(\partial\tilde{\Omega}_{\text{eff}}/\partial\omega_B)_{T\mu}$, which contains the trigonometric functions of $2\pi p\mu/\omega_+$ and $2\pi p\mu/\omega_-$. It should be noted that as the temperature T decreases, the amplitude of the oscillation of \tilde{M} becomes larger.

In the following, we discuss how the three regions introduced by IF [3] are modified in 3D. We regard the LD region as the region where the amplitudes of the oscillations specified by p are much smaller than the confining energy $\hbar\omega_3$, which is unity in our notation. Hence, the criterion for the LD region is given by $|Q_2^{\pm}(p)|\Psi(2p\pi^2T/\omega_{\pm}) \ll 1$ for all p . Introducing the cutoff $\epsilon (\ll 1)$, we defined the LD region as the region where the following two inequalities hold simultaneously,

$$\Psi(2p\pi^2T/\omega_+) \leq \epsilon, \quad \Psi(2p\pi^2T/\omega_-) \leq \epsilon. \quad (20)$$

In this letter, we set $\epsilon = 0.1\%$, but it will be necessary, however, to reexamine the value of ϵ when our analytic classification is compared to any experiment. Noting

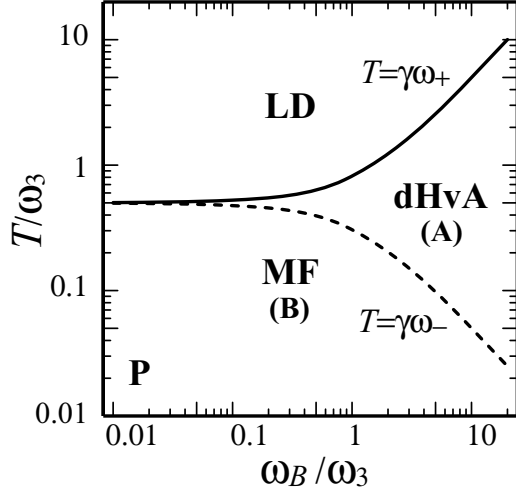


FIG. 1: Temperature-field (T - B) plane can be classified into three regions: the Landau diamagnetism (LD), the de Haas-van Alphen (dHvA) oscillation, and the mesoscopic fluctuation (MF), in terms of the characteristic behavior of the magnetization $M(T, B)$. ω_B is the cyclotron frequency and ω_3 parametrizes the strength of the confinement. In the region indicated by P, the remarkable paramagnetism appears.

$\Psi'(x) < 0$ and $\omega_+ > \omega_-$, the region determined by eq. (20) is equivalent to $T \geq \gamma\omega_+$, where $\gamma = \Psi^{-1}(\epsilon)/(2\pi^2) \approx 0.5$. As a result, the boundary between the LD and the oscillatory region is given by $T = 0.5\omega_+$, as plotted by the solid line in Fig.1.

The oscillatory region $T < \gamma\omega_+$ is divided into two subregions as shown in Fig.1; (A) $\gamma\omega_+ > T \geq \gamma\omega_-$, and (B) $\gamma\omega_- > T$. In subregion (A), the first inequality in eq. (20) fails while the second one still holds. Hence, only $Q_2^+(p)\Psi(2\pi^2T/\omega_+)\cos(2\pi\mu/\omega_+)$ contributes to $\tilde{\Omega}_{\text{eff}}$. The effective free energy $\tilde{\Omega}_{\text{eff}}^A$ is given by $\tilde{\Omega}_{\text{eff}}^A = \sum_{p=1}^{\infty} Q_2^+(p)\Psi(2p\pi^2T/\omega_+)\cos(2p\pi\mu/\omega_+)$. On the other hand, both inequalities fail in subregion (B), where two types of oscillations regarding ω_{\pm} contribute to $\tilde{\Omega}_{\text{eff}}$, and the free energy $\tilde{\Omega}_{\text{eff}}^B$ is given by eq. (14). As the temperature T is lowered, the terms with larger p start contributing to $\tilde{\Omega}_{\text{eff}}$.

For subregion (A), magnetization \tilde{M} derived from $\tilde{\Omega}_{\text{eff}}^A$ contains a trigonometric function having the period ω_+/μ . The dHvA region corresponds to the region $\gamma\omega_- \leq T < \gamma\omega_+$, characterized by the oscillation having the period ω_+/μ . Particularly in a strong field region, since $\omega_+ \sim \omega_B$, magnetization \tilde{M} behaves as the periodic function of variable ω_B^{-1} . This periodicity is typical of the dHvA oscillation in a bulk system. [8, 9]

For subregion (B), magnetization \tilde{M} derived from $\tilde{\Omega}_{\text{eff}}^B$ contains a trigonometric function having the period ω_-/μ in addition to ω_+/μ . In this region, ω_+ and ω_- are not so close to each other and the two modes fluctuate separately. Consequently, the coexistence of the above two modes causes the rapid and irregular oscillation of magnetization. This magnetic behavior corresponds to the MF. Hence, subregion (B) is regarded as the MF region.

However, when the magnetic field is extremely weak in the MF region, the periods of ω_{\pm}/μ become much closer since $\omega_{\pm} \sim 1 \pm \frac{1}{2}\omega_B$. It is impossible to regard ω_{\pm} as distinguishable and therefore the separation of the two fluctuations breaks down in the above argument. In this case, the largest contribution to $\tilde{\Omega}$ in eq. (15) comes from the modes satisfying $p : q : r = \omega_1 : \omega_2 : \omega_3$, namely, $p/\omega_1 - q/\omega_2 = q/\omega_2 - r/\omega_3 = r/\omega_3 - p/\omega_1 = 0$ for $\hat{\Omega}_{p,q,r}^{\sigma}$ in eq. (18). From the behavior of characteristic frequency $\omega_1 \sim 2 + \frac{1}{4}\omega_B^2$, we can see that the modes of $p = 2j$, $q = j$, $r = j$ (j is a natural number) make a dominant contribution to magnetization \tilde{M} . The largest contribution to \tilde{M} is evaluated as

$$\frac{\tilde{M}}{\mu_B} \sim \sum_{j=1}^{\infty} \frac{\hat{M}_{2j,j,j}}{\mu_B} = -2 \sum_{\sigma=\pm} \sum_{j=1}^{\infty} \left(\frac{\partial \hat{\Omega}_{2j,j,j}^{\sigma}}{\partial \omega_B} \right)_{T\mu}. \quad (21)$$

Furthermore, we can estimate the upper bound $U(p, q, r)$ of $|\hat{\Omega}_{p,q,r}^{\sigma}|$ by using the triangle inequality and $|Y(x)| \leq 1$ for eq.(18), and it is found that the upper bound $U(2j, j, j)$ decreases as $U(2j, j, j) = j^{-4}U(2, 1, 1)$ for larger j . Hence, it is expected that a few modes with small j make a major contribution. The mode with $j = 1$, $\hat{M}_{2,1,1}$, is plotted in Fig.2(a), where we take $T = 0.01$ and $N = 5000$. The magnetization curve in Fig.2(a) shows a remarkable paramagnetism at weak magnetic fields below $\omega_B \sim 0.02$. The region corresponding to the paramagnetism is indicated by P in Fig.1.

Next, we describe the procedure of the numerical calculation for magnetization. We consider magnetization as the total dipole moment of electrons with the confining potential. From this standpoint, magnetization \mathbf{M} is given by $\mathbf{M} = \int_{\infty} dV \frac{1}{2} [\mathbf{r} \times \mathbf{J}(\mathbf{r})]$, where $\mathbf{J}(\mathbf{r})$ is the current density distribution of the system. The calculation of \mathbf{M} reduces to that of $\mathbf{J}(\mathbf{r})$ which is given by $\mathbf{J}(\mathbf{r}) = \text{Re} \sum_{s=(n,\alpha,\nu)} f(E_s) \psi_s^*(\mathbf{r}) \frac{-e}{m} (-i\nabla + e\mathbf{A}) \psi_s(\mathbf{r})$. Here, $f(E)$ denotes the Fermi distribution function, $f(E) = \{\exp[(E - \mu)/T] + 1\}^{-1}$. By using eq.(2), the current density distribution leads to $\mathbf{J}(\mathbf{r}) = J(\rho, z)\mathbf{e}_{\phi}$, and

$$J(\rho, z) = -\sqrt{\frac{e}{m}} \sum_{s=(n,\alpha,\nu)} f(E_s) |\psi_s(\mathbf{r})|^2 \left(\alpha \frac{\xi}{\rho} + \frac{\omega_B \rho}{2} \frac{1}{\xi} \right), \quad (22)$$

where $\xi = m^{-\frac{1}{2}}$. By using eq.(22), the total dipole moment \mathbf{M} is calculated analytically [3] and then $\mathbf{M} = M\mathbf{e}_z$. The z -component M is given by

$$M/\mu_B = - \sum_{s=(n,\alpha,\nu)} f(E_s) [\alpha + (2n + |\alpha| + 1) \omega_B/\omega_1], \quad (23)$$

which is also derived from $M/\mu_B = -2(\partial\Omega/\partial\omega_B)_{T\mu} = -2 \sum_s f(E_s)(\partial E_s/\partial\omega_B)$ due to eq.(3). This coincidence of two derivations, of course, occurs regardless of the type of confining potentials. In the numerical calculation, we calculate the chemical potential first by solving $N = \sum_s f(E_s)$ for μ , and then compute magnetization M by using eq.(23).

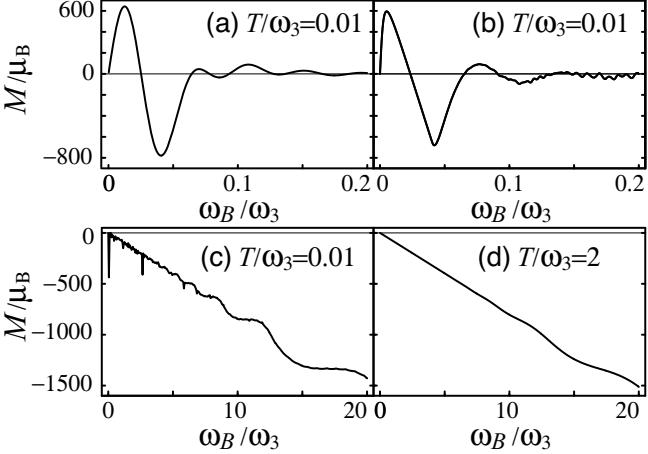


FIG. 2: Figure 2(a) shows the contribution $\hat{M}_{2,1,1}$, which is the lowest mode ($j = 1$) in eq. (21). Figures 2(b)-2(d) show the magnetization curve obtained by the numerical calculation for $N = 5000$.

Magnetization M calculated numerically is shown in Fig.2 for $N = 5000$. At low temperatures ($T = 0.01$, Figs.2(b) and 2(c)), the magnetization oscillates over the entire range of magnetic fields. At extremely weak fields below $\omega_B \sim 0.1$ (Fig.2(b)), the magnetization oscillates smoothly with significantly large amplitude. The smoothness implies that not so many modes are dominant in the oscillation. Moreover, Fig.2(b) agrees qualitatively with the behavior of $\hat{M}_{2,1,1}(T, \mu, B)$ (Fig.2(a)) with the chemical potential $\mu(T, N, B)$ calculated numerically for $T = 0.01$ and $N = 5000$. The large smooth oscillation in Fig.2(b) is consistent with our analysis in terms of free energy. At weak magnetic fields above $\omega_B \sim 0.1$, the large oscillation is suppressed and the magnetization irregularly takes a positive or negative value. This fluctuation continues until $\omega_B \sim 5$ with the linear magnetization superposed (Fig.2(c)). At high magnetic fields above $\omega_B \sim 5$, the large smooth oscillation is clear in Fig.2(c). It is considered that this magnetization curve reflects the dHvA oscillation. On the other hand, at high temperatures ($T = 2$, Fig.2(d)), the magnetization is linear in ω_B until $\omega_B \sim 10$ and then the dHvA oscillation increases gradually.

Compared with the magnetization in 2D reported by IF, [3] it is found that the period of oscillation is longer in 3D. For the 2D system, they also calculated the free energy analytically and its oscillating part is expressed as $\Omega = \sum_{i=1}^2 \sum_{\sigma} \sum_p \Omega_i^{\sigma}(p)$, and $\Omega_i^{\sigma}(p) = Q_i^{\sigma}(p) \Psi(2p\pi^2 T/\omega_i) \sin(2p\pi\mu/\omega_i)$, in our notation. Here, we find that for 2D and 3D, these oscillating factors have the common phase $2p\pi\mu/\omega_i$. Noting the common phase, when ω_B is varied, the period with respect to ω_i^{-1} , $\Delta(1/\omega_i)$, is given by $\Delta(1/\omega_i) = p^{-1}\mu^{-1}$. Hence, μ^{-1} serves as the scale for the period of oscillation and the difference between the periods can be explained by that between the chemical potentials. The chemical poten-

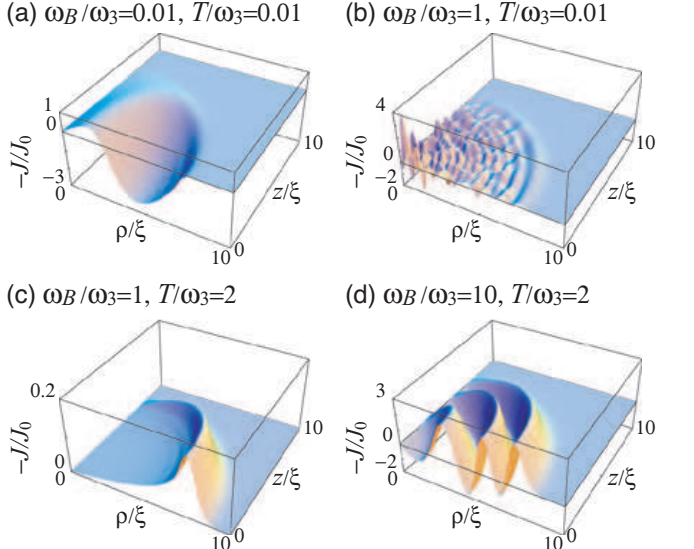


FIG. 3: Figures 3(a)-3(d) show the current density distribution $J(\rho, z)$ for $N = 5000$ obtained by the numerical calculation. ρ is radius and z is height parallel to the magnetic field \mathbf{B} . Here, $\xi = 1/\sqrt{m\omega_3}$ and $J_0 = e\omega_3/(4\pi\xi^2)$. Four figures correspond to the characteristic regions of magnetization.

tials μ_{3D}, μ_{2D} are estimated by $N \approx -(\partial\Omega_0/\partial\mu)_{TB}$ and then $\mu_{3D} \approx \sqrt[3]{6N} < \mu_{2D} \approx \sqrt{2N}$ for the same number of electrons. Consequently, the period of oscillation in 3D is longer than that in 2D.

The current density distribution $J(\rho, z)$ is computed by using eq.(22) and is shown in Fig.3 for $N = 5000$. The positive value of the vertical axis corresponds to diamagnetism. When the remarkable paramagnetism appears (Fig.3(a)), a paramagnetic region for $J(\rho, z)$ extends throughout the spherical quantum dot except for a small region near the z -axis ($\rho = 0$). In the MF region (Fig.3(b)), the paramagnetic and diamagnetic regions are distributed irregularly. In the LD region (Fig.3(c)), the current density distribution is localized near the surface of the quantum dot. This surface current corresponds to the edge current obtained by IF [3] for the 2D system. In the dHvA region (Fig.3(d)), the current density distribution oscillates smoothly with a large amplitude.

In conclusion, we have studied orbital magnetism in a 3D quantum dot with a parabolic confining potential. From the analysis of the free energy, we have determined the boundaries between the LD, dHvA, and MF regions. We have also computed the magnetization of the system and then the current density distribution, which indeed reflects the character of each region. The results of numerical calculation show a large paramagnetism when the magnetic fields are extremely weak in the MF region. The dHvA oscillation has a longer period in 3D than that in a 2D quantum dot. These results are explained in terms of the free energy. Furthermore, we have found surface current in the LD region, corresponding to edge current for 2D quantum dots.

The authors are grateful to H. Fukuyama and T. Sasaki for their useful discussions. H. I. is supported by MEXT,

Grant-in-Aid for Encouragement of Young Scientists, 13740197.

- [1] J. H. van Vleck: *The Theory of Electric and Magnetic Susceptibilities* (Clarendon Press, Oxford, 1932) §26.
- [2] R. Peierls: *Surprises in Theoretical Physics* (Princeton University Press, New Jersey, 1979) §4.3.
- [3] Y. Ishikawa and H. Fukuyama: J. Phys. Soc. Jpn. **68** (1999) 2405.
- [4] The theoretical studies on effects of boundary are listed in the reference of the above paper. [3]
- [5] S. Tarucha, D. G. Austing, T. Honda, R. J. van der Hage and L. P. Kouwenhoven : Phys. Rev. Lett. **77** (1996) 3613.
- [6] R. C. Ashoori: Nature (London) **379** (1996) 413.
- [7] S. Tarucha, T. Honda, D. G. Austing, Y. Tokura, K. Murakami, T. H. Oosterkamp, J. W. Janssen and L. P. Kouwenhoven : Physica (Amsterdam) **3E** (1998) 112.
- [8] L. D. Landau and E. M. Lifshitz: *Statistical Physics, Part 2*, (Pergamon, Oxford, 1980) §63.
- [9] L. D. Landau and E. M. Lifshitz: *Statistical Physics, Part 1*, (Pergamon, Oxford, 1980) §59, §60.